Flat-band engineering of mobility edges

Carlo Danieli,[1] Joshua D. Bodyfelt,[1] and Sergej Flach[1,2]

[1]*New Zealand Institute for Advanced Study, Centre for Theoretical Chemistry & Physics, Massey University, Auckland, New Zealand*

[2]*Center for Theoretical Physics of Complex Systems, Institute for Basic Science, Daejeon, Korea*

(Received 24 February 2015; revised manuscript received 5 June 2015; published 19 June 2015)

Properly modulated flat-band lattices have a divergent density of states at the flat-band energy. Quasiperiodic modulations are known to host a metal-insulator transition already in one space dimension. Their embedding into flat-band geometries consequently allows for a precise engineering and fine tuning of mobility edges. We obtain analytic expressions for singular mobility edges for two flat-band lattice examples. In particular, we engineer cases with arbitrarily small energy separations of mobility edge, zeroes, and divergencies.

DOI: 10.1103/PhysRevB.91.235134 PACS number(s): 71.10.−w, 71.30.+h, 72.20.Ee

I. INTRODUCTION

The phenomenon of wave localization has been intensively studied since its prediction in 1958 [1], where complete localization was proved in the case of a one-dimensional (1-D) chain defined over a random potential. Moreover, it was shown that the 3-D case allows for an energy-dependent transition from localized to delocalized eigenstates. The transition has been since coined metal-insulator transition (MIT). The critical energy E_c is called a mobility edge; in general, it depends on and varies upon changes of the control parameters of the given model [2]. Interestingly, an MIT can also be realized in one-dimensional settings with sufficiently correlated disorder potentials [3].

In 1980, Aubry and André proved the existence of the MIT for a 1-D chain defined over a specific quasiperiodic potential [4]. This MIT occurs at a critical value ($\lambda_c = 2$) of the on-site potential's strength λ, and separates the metallic phase $\lambda \in]0,2[$ from an insulating phase $\lambda \in]2,+\infty[$. This remarkable result was fully understood via the principle of duality, in which a particular Fourier transformation relating eigenmodes and energy spectra allows for a direct functional equivalency between momentum space and its transform counterpart. This equivalency is energy-independent: upon crossing the critical value λ_c all eigenstates turn from localized to extended, regardless of their eigenenergy. The appearance of a mobility edge is thus avoided. Analytic results have been discovered in the last decade regarding the topological Cantor structure of the spectrum [5] and its Lebesgue measure [6]. Furthermore, for each different regime (insulating, metallic, and critical) different spectral decompositions have been found [7–9]. Model generalizations were reported, e.g., quasiperiodic systems constantly maintained at criticality [10,11], bichromatic quasiperiodic lattices displaying mobility edges [12,13], and completely localized quasiperiodic models [14]. Correlated metallic states have also been observed in the insulating regime, for the case of two interacting particles within a 1-D Aubry-André chain [15]. In another recent work [16], a suitably modified quasiperiodic potential was shown to produce a mobility edge expressible in an analytic form—a property which we will take to new limits using flat-band topologies.

Wave propagation on lattices with flat-band topologies is characterized by the existence of horizontal (flat) bands in their band structure. Known in condensed matter, this model class has gained great interest in the scientific community, due in part to experimental realizations in optical lattices and paraxially approximate light propagations [17–19]. Recent theoretical discoveries have also considered the presence of a disordered potential [20,21] and nonlinearity [22]. An innovative procedure detangles flat-band states from dispersive ones [23]. This allows one to inspect specific features of the models as they relate to the choice of the on-site perturbations, and also suggests specific potential correlations. In the present work, this detangling technique of local rotations [23] is applied as an extension of [25], in particular, regarding the preliminary finding of an MIT occurring in a flat-band lattice under quasiperiodic Aubry-André perturbation.

The present paper has the following structure: In Sec. II the general features of flat-band topologies are introduced that define two particular models (cross-stitch and diamond lattices), a quasiperiodic Aubry-André on-site perturbation is defined, and the coordinate transformation that allows rotation into Fano defect lattices [23]. In Secs. III and IV, our findings for the cross-stitch and diamond lattices are respectively presented: for both, two distinct chain correlations are discussed. Where applicable, the exact mathematical expression obtained for the mobility edge is jointly shown with numerically obtained transitions for these particular on-site correlations.

II. FLAT-BAND TOPOLOGIES

Consider the eigenvalue problem of a generalized tight-binding model:

$$E\psi_n = \epsilon_n\psi_n - \hat{V}\psi_n - \hat{T}\psi_{n-1} - \hat{T}^\dagger\psi_{n+1}. \qquad (1)$$

For all $n \in \mathbb{Z}$, each component of the vector $\psi_n = (\psi_n^1, \ldots, \psi_n^\ell)^T$ represents a site of a periodic lattice, while the set of sites represented by ψ_n is the nth unit cell. The real matrix $\hat{V}$ defines the geometry of the unit cell, while the real matrix $\hat{T}$ describes hopping to neighboring cells (as will be clarified below for each model). At each of the lattice's ith leg $\{\psi_n^i\}_n$, an on-site perturbation $\{\epsilon_n^i\}_n$ is defined. The unit cell perturbation ϵ_n of Eq. (1) is thus given by the diagonal square matrix $\epsilon_n = \mathrm{diag}(\epsilon_n^a, \epsilon_n^b, \ldots, \epsilon_n^\ell)$.

The model geometry is contained in the matrices $\hat{T}$ and $\hat{V}$, which are then used to derive the dispersion spectrum via the Bloch solution $\psi_n = \phi_k e^{ikn}$ on an unperturbed crystal $\epsilon_n = 0$. Flat-band topologies are models in which this crystalline case exhibits *at least* one band independent of k; such a

 ©2015 American Physical Society

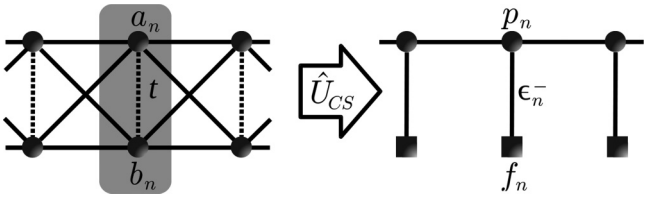

FIG. 1. Left: The cross-stitch lattice. The gray-shaded region indicates the unit cell. Right: The transformed Fano defect lattice of Eq. (10).

band is dispersionless, or "flat". Eigenmodes corresponding to this flat-band energy are (usually) compact localized states (CLS), i.e., modes whose amplitude is nonzero only across a finite number of sites [23]. The flat-band topology class U is then defined as the minimum number of unit cells the CLS occupies [23].

In this paper we consider two lattice topologies, the cross-stitch and diamond. Both are examples of "frustrated two-leg ladders", which have garnered intense interest from the quantum spin chain community [24]. The cross-stitch model, shown on the left of Fig. 1, is defined for a unit cell $\psi_n = (a_n,b_n)^T$ with a 2×2 perturbation matrix ϵ_n. This yields for Eq. (1) the following matrices:

$$\hat{V}_{CS} = \begin{pmatrix} 0 & t \\ t & 0 \end{pmatrix}, \quad \hat{T}_{CS} = \begin{pmatrix} 1 & 1 \\ 1 & 1 \end{pmatrix}. \tag{2}$$

Likewise for the diamond lattice, as shown on the left of Fig. 2, the unit cell is $\psi_n = (a_n,b_n,c_n)^T$ with a 3×3 perturbation matrix ϵ_n. In this case, the matrices in Eq. (1) are

$$\hat{V}_{DC} = \begin{pmatrix} 0 & t & 1 \\ t & 0 & 1 \\ 1 & 1 & 0 \end{pmatrix}, \quad \hat{T}_{DC} = \begin{pmatrix} 0 & 0 & 0 \\ 0 & 0 & 0 \\ 1 & 1 & 0 \end{pmatrix}. \tag{3}$$

In the unperturbed crystal $\epsilon_n = 0$, the dispersive bands are

$$E(k) = \begin{cases} -t - 4\cos k, & \text{cross-stitch,} \\ -\frac{1}{2}(t \ pm \sqrt{t^2 + 16\cos k + 16}), & \text{diamond.} \end{cases} \tag{4}$$

Additionally, both models contain a flat band at $E(k) = t$.

Associated with the flat-band energy, resulting compact localized states (CLS) can be constructed: $\psi_n = (1,-1)^T\delta_{n,n_0}/\sqrt{2}$ (cross-stitch) and $\psi_n = (1,-1,0)^T\delta_{n,n_0}/\sqrt{2}$ (diamond). Note that both CLS are contained within a single unit cell. Therefore, according to the definition previously stated, both lattices are flat-band models class $U = 1$. Coordinate transformations local to the unit cells rotate these lattices into a Fano defect form [23]. For the cross-stitch, the rotation

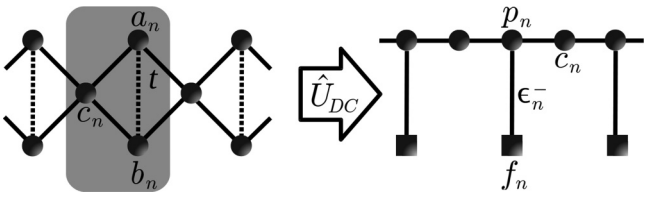

FIG. 2. Left: The diamond lattice. The gray-shaded region indicates the unit cell. Right: The transformed Fano defect lattice of Eq. (21).

is defined by the real matrix $\hat{U}_{CS}$

$$\begin{pmatrix} p_n \\ f_n \end{pmatrix} = \hat{U}_{CS}\ \psi_n, \quad \hat{U}_{CS} = \frac{1}{\sqrt{2}}\begin{pmatrix} 1 & 1 \\ 1 & -1 \end{pmatrix}. \tag{5}$$

Similarly for the diamond lattice the transformation is defined by the real matrix $\hat{U}_{DC}$

$$\begin{pmatrix} p_n \\ f_n \\ c_n \end{pmatrix} = \hat{U}_{DC}\ \psi_n, \quad \hat{U}_{DC} = \frac{1}{\sqrt{2}}\begin{pmatrix} 1 & 1 & 0 \\ 1 & -1 & 0 \\ 0 & 0 & \sqrt{2} \end{pmatrix}. \tag{6}$$

Lastly, this local coordinate transformation must also rotate the on-site perturbation. For both lattices, this gives

$$\epsilon_n^{\pm} = \left(\epsilon_n^a \pm \epsilon_n^b\right)/2. \tag{7}$$

The effect of quasiperiodic Aubry-André perturbations on these two topologies is the focus of the present work. For both lattices, the on-site perturbations $\{\epsilon_n^i\}$ are defined as *independent* Aubry-André potentials

$$\epsilon_n^i = \lambda_i \cos[2\pi(\alpha n + \theta_i)], \tag{8}$$

for the $i = a,b$ (cross-stitch) and $i = a,b,c$ (diamond) legs. The parameters λ_i are positive real values controlling the perturbative strength, θ_i is the phase shift, and α is an irrational number (here set to the golden ratio) called the *incommensurate parameter*. Without loss of generality, the a-leg phase can be zeroed ($\theta_a = 0$). We also set the leg potential strengths equal to each other $\lambda_i = \lambda$.

From Eq. (7), notable correlations between the a-leg and b-leg perturbations appear and will be the object of our studies for both models; namely

$$\begin{aligned} \text{symmetric:} \quad & \epsilon_n^- = 0 \Leftrightarrow \epsilon_n^a = \epsilon_n^b, \\ \text{antisymmetric:} \quad & \epsilon_n^+ = 0 \Leftrightarrow \epsilon_n^a = -\epsilon_n^b. \end{aligned} \tag{9}$$

Since the a-leg phase has been zeroed, from Eq. (8) these two correlations are obtained solely from the b-leg phase; e.g., $\theta_b = 0.5$ ($\theta_b = 0$) for the antisymmetric (symmetric) case.

Note that in the crystalline case $\epsilon_n = 0$, the number of bands in the dispersion relation equals the number of sites in the unit cell for each of the above models, Eq. (4). Breaking the translation invariance of the lattices with the introduction of a nonperiodic on-site perturbation [e.g., Eq. (8)] will generally lead to a loss of the spectral band structure due to hybridization, resulting in one single energy spectrum for the model. However as seen here, the symmetric case of Eq. (9) renormalizes the flat-band states, yet keeps their compact localized form due to the absence of any hybridization with the rest of the dispersive states. Note that the resulting eigenstate separation into two groups (CLS and dispersive) is unrelated to the above-mentioned band structure of the crystalline case, since the spectra of both groups will overlap in general. We start the analysis of these models with the cross-stitch in Sec. III, and then with the diamond lattice in Sec. IV.

III. CROSS-STITCH LATTICE

By Eqs. (5) and (7), the cross-stitch lattice transforms into

$$\begin{aligned} (E+t)\ p_n &= \epsilon_n^+\ p_n + \epsilon_n^-\ f_n - 2(p_{n-1} + p_{n+1}), \\ (E-t)\ f_n &= \epsilon_n^+\ f_n + \epsilon_n^-\ p_n. \end{aligned} \tag{10}$$

This results in a Fano chain, as shown in the right of Fig. 1. The local rotation yields a dispersive coordinate p_n and a compact Fano coordinate f_n. The sequence ϵ_n^+ describes on-site perturbations of both p_n and f_n, while the sequence ϵ_n^- couples the dispersive to the Fano coordinate within the rotated unit cell [23]. Solving for the Fano coordinates f_n in the second equation above, we obtain a new equation for the dispersive portion,

$$(E+t)\,p_n = \left[\epsilon_n^+ + \frac{(\epsilon_n^-)^2}{(E-t)-\epsilon_n^+}\right] p_n - 2(p_{n-1}+p_{n+1}). \tag{11}$$

The reduced topology assumes the tight-binding form. If eigenmodes are exponentially localized, their asymptotic decay is $\psi_n^\nu \sim e^{-\frac{n}{\xi}}$. The rate $\xi^{-1}(E)$ is the inverse localization length of a localized state at eigenenergy $E \in \mathbb{R}$, found by applying the recursive iteration

$$\xi^{-1}(E,\lambda) = \lim_{M\to+\infty} \frac{1}{M} \sum_{n=1}^{M} \ln\left|\frac{p_{n+1}}{p_n}\right| \tag{12}$$

for any given potential strength λ. We will use this method in all the numerical computations of the two models' localization lengths, for $M = 10^6$. The energy E in Eq. (11) will be numerically found from an exact diagonalization of a finite lattice of $N = 512$ unit cells. In all the figures of the paper, if the recursive iteration converges to a finite value (chosen [26] here as $\xi \leqslant N/10$), the data point (E,λ) is declared a localized state and plotted in blue. Otherwise if the iteration diverges, the data point is declared an extended state and plotted in red.

A. Symmetric case: Metal-insulator transition

We analyze first the symmetric case $\epsilon_n^- = 0$, obtained for $\theta_b = 0.0$. Equation (10) reads

$$\begin{aligned}(E+t)\,p_n &= \epsilon_n^+\,p_n - 2(p_{n-1}+p_{n+1}),\\ (E-t)\,f_n &= \epsilon_n^+\,f_n,\end{aligned} \tag{13}$$

with $\epsilon_n^+ = \epsilon_n^i$. The two sets of states p_n and f_n decouple and generate two independent spectra, respectively labeled σ_p and σ_f. The parameter t then simply operates as a shift parameter, translating σ_p and σ_f relative to each other by $2t$.

The dispersive states p_n are described by an Aubry-André chain, displaying an MIT at $\lambda_c = 4$. The σ_f states keep their compact feature, but the degeneracy of their eigenenergies is now removed; these eigenenergies are given by $E = \epsilon_n^+ + t$. In Fig. 3, we plot the spectrum from Eq. (13), as a function of λ. In this symmetric case, the spectra σ_p and σ_f are independent, since the p_n and the f_n coordinates decouple. For every potential strength $\lambda > 0$, the Fano states spectrum $\sigma_f = \{\epsilon_n^+\}_n$ is equidistributed within the interval $[t-\lambda, t+\lambda]$. In Fig. 3 we indicate its boundaries by dashed lines. For the dispersive spectrum σ_p, the localization length is numerically found with the recursive iteration (12), and the localized phase (red) is demarcated from the extended one (blue). At the critical value $\lambda_c = 4$, all dispersive states switch from extended to localized. In this case, there is no mobility edge.

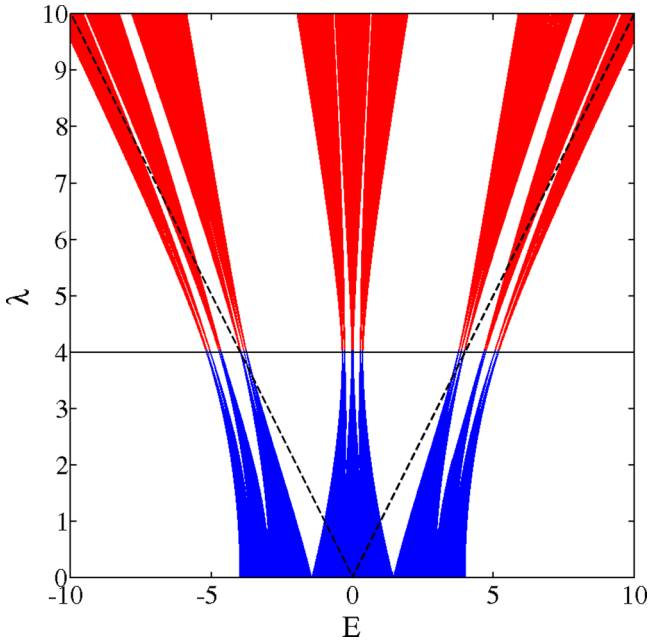

FIG. 3. (Color online) Symmetric case. The dispersive spectrum (σ_p) of the cross-stitch lattice, for $\epsilon_n^- = 0$ and $t = 0$. The Fano state spectrum σ_f is omitted, but its boundaries are indicated by black dashed lines. The black line represents the MIT at $\lambda = 4$, which clearly separates extended states (blue) from those localized (red).

B. Asymmetric case $\epsilon_n^- \neq 0$: Numerical evidence for mobility edge

Breaking the symmetry $\epsilon_n^- \neq 0$ ($\theta_b \neq 0$) of the Fano chain Eq. (10) effectively couples the dispersive states p_n to their compact Fano counterparts f_n. Therefore, the self-duality is lost, and the two independent spectra ($\sigma_{p,f}$) are now joint. Nevertheless, we expect a transition between localized and extended states via an energy-dependent mobility edge. In Fig. 4 we plot the spectrum of the lattice in the asymmetric case for $\theta_b = 0.25$ and $t = 0$. A mobility edge is clearly observed separating the localized regime (red) from that which is extended (blue).

C. Antisymmetric case ($\epsilon_n^+ = 0$): Analytic mobility edge

Among all the nonsymmetric cases obtained for $\theta_b \neq 0$, antisymmetry ($\theta_b = 0.5$) deserves special attention. It was already introduced in [25], providing a starting point in which to clarify technical details and to obtain a closed form for mobility edge curves; this will be made use of later on for discussion of the diamond chain.

In this situation $\epsilon_n^+ = 0$ and Eq. (10) transforms into

$$\begin{aligned}(E+t)\,p_n &= \epsilon_n^-\,f_n - 2(p_{n-1}+p_{n+1}),\\ (E-t)\,f_n &= \epsilon_n^-\,p_n.\end{aligned} \tag{14}$$

Since $\epsilon_n^- \neq 0$, from the second equation of (14) it follows that at the flat-band energy

$$\epsilon_n^-\,p_n = 0 \quad \Rightarrow \quad p_n = 0. \tag{15}$$

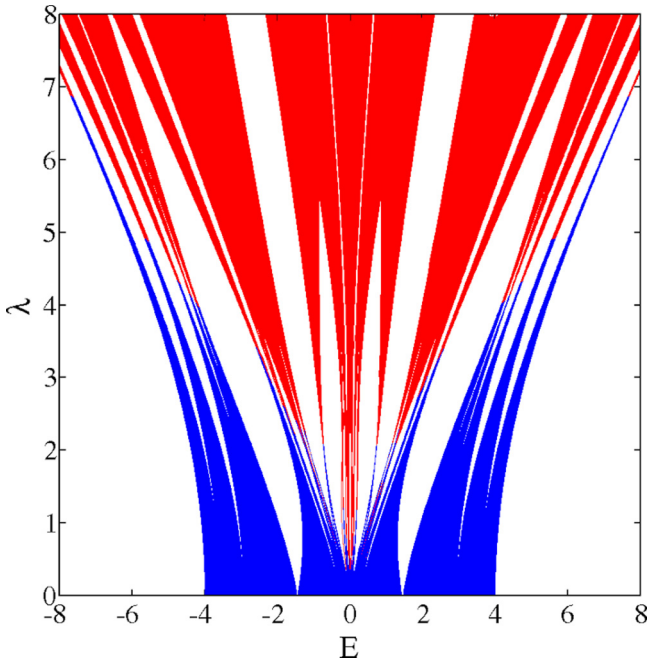

FIG. 4. (Color online) Asymmetric case. Spectrum of the cross-stitch lattice, for $\theta = 0.25$ and $t = 0$. The extended (localized) portion of the spectrum is shown in blue (red), while the color boundary is a mobility edge approximation of the spectrum.

Then, from the first equation of (14) we conclude

$$\epsilon_n^- \, f_n = 0 \quad \Rightarrow \quad f_n = 0. \tag{16}$$

Therefore, only $(p_n, f_n) = (0,0)$ satisfies Eq. (14) exactly at the flat-band energy $E = t$. It follows that all compact localized states are expelled from the unperturbed flat-band energy $E = t$, since their energies are shifted away from this energy due to hybridization with the dispersive states. The resulting states are then localized modes, located in the localized portion of the energy spectrum.

As already observed in [25], for this case we identify the analytical form of the mobility edge. Indeed the dispersive part, Eq. (11), reads

$$(E + t)\, p_n = \frac{(\epsilon_n^-)^2}{E - t}\, p_n - 2(p_{n-1} + p_{n+1}). \tag{17}$$

By trigonometric bisection

$$(\epsilon_n^-)^2 = \lambda^2 \cos^2(2\pi\alpha n) = \frac{\lambda^2}{2}[1 + \cos(4\pi\alpha n)]. \tag{18}$$

Substituting Eq. (18) back into the previous equation, we obtain

$$\tilde{E}\; p_n \;=\; \frac{\lambda^2}{4(E - t)} \cos(4\pi\alpha n) - (p_{n-1} + p_{n+1}),$$
$$\text{where } \tilde{E} := \frac{E + t}{2} - \frac{\lambda^2}{4(E - t)}. \tag{19}$$

Therefore, the model becomes an Aubry-André chain eigenequation, but with on-site perturbation strength depending on λ and E. From [4], the MIT occurs when the potential strength is twice larger than the hopping strength. Imposing that condition, an analytic expression is found for the mobility edge, $\lambda_c(E_c)$:

$$\left|\frac{\lambda_c^2}{4(E_c - t)}\right| = 2 \quad \Rightarrow \quad \lambda_c(E_c) = 2\sqrt{2|E_c - t|}. \tag{20}$$

Note that for $E_c = t$, the critical potential strength λ_c vanishes in a square root manner, where the previously discussed lack of states at the unperturbed flat-band energy $E = t$ occurs. The analytic curve of the mobility edge was already plotted in Fig. 4 of [25], displaying excellent agreement with the numerical result.

IV. DIAMOND LATTICE

Under the transformation in Eqs. (6) and (7), the diamond lattice's Eq. (1) becomes

$$\begin{aligned}(E + t)\, p_n &= \epsilon_n^+ p_n + \epsilon_n^- f_n - \sqrt{2}(c_n + c_{n+1}),\\ (E - t)\, f_n &= \epsilon_n^+ f_n + \epsilon_n^- p_n,\\ \left(E - \epsilon_n^c\right) c_n &= -\sqrt{2}(p_{n-1} + p_n),\end{aligned} \tag{21}$$

as illustrated graphically in the right plot of Fig. 2. Expressing the f_n and c_n variables through the p_n ones we reduce these equations to a tight-binding form which contains the p_n coordinates only:

$$\begin{aligned}(E + t)p_n &= \left[\epsilon_n^+ + \frac{(\epsilon_n^-)^2}{(E - t) - \epsilon_n^+} + \frac{2}{E - \epsilon_n^c} + \frac{2}{E - \epsilon_{n+1}^c}\right] p_n\\ &\quad + \frac{2}{E - \epsilon_n^c} p_{n-1} + \frac{2}{E - \epsilon_{n+1}^c} p_{n+1},\\ &= \tilde{\epsilon}_n\, p_n + \gamma_{n-1}\, p_{n-1} + \gamma_{n+1}\, p_{n+1}.\end{aligned} \tag{22}$$

The effective on-site potential $\tilde{\epsilon}_n$ is a function of the three on-site energies of the diamond lattice $\epsilon_n^{a,b,c}$ in Eq. (8). However, the effective hopping terms $\gamma_{n\pm1}$ depend only on the on-site energy ϵ_n^c of the c chain. Since the model has both quasiperiodic on-site energies and hopping coefficients, one may expect that the Aubry-André duality does not generally hold.

Also note that the functional dependence of several terms in Eq. (22) is of the form

$$\frac{2}{E - \epsilon_n^c} = \frac{2}{E - \lambda\cos[2\pi(\alpha n + \theta_c)]}, \tag{23}$$

which was used in Ref. [16] for a model with constant hopping coefficients to arrive at analytically expressible mobility edges. Therefore one can expect that mobility edges will be present in our model as well. As an example, in Fig. 5 the spectrum of the diamond lattice Eq. (22) is plotted, for $\theta_b = 0.5, \theta_c = 0.05$, and $t = 0$; a mobility edge is clearly observed.

To obtain closed forms of the mobility edge, the hopping terms are set constant: $\gamma_{n\pm1} = \Gamma$. From Eq. (23), this choice corresponds to

$$\frac{2}{E - \epsilon_n^c} = \Gamma \quad \Leftrightarrow \quad \epsilon_n^c = K \tag{24}$$

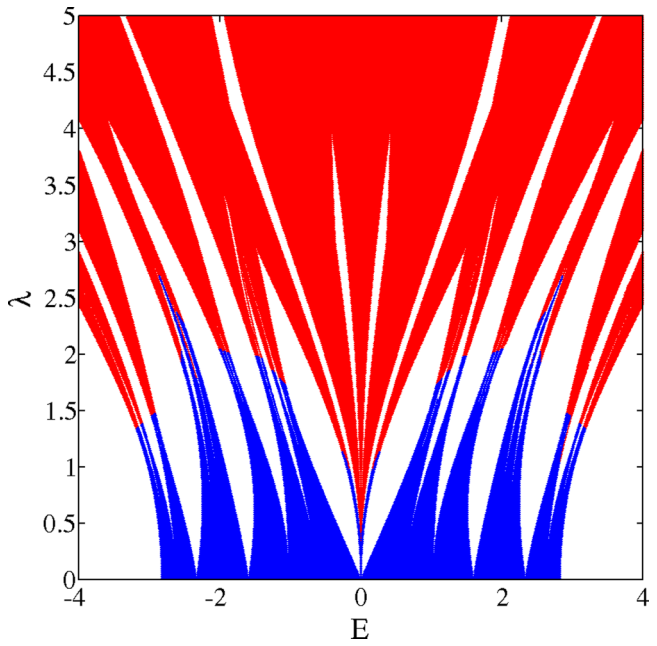

FIG. 5. (Color online) Spectrum of the diamond lattice, for $\theta_b = 0.5$, $\theta_c = 0.05$, and $t = 0$. The extended (localized) spectral portion is shown in blue (red), while the color boundary is again a spectral mobility edge approximation.

for a real constant value K. Equation (22) becomes

$$(E+t)\,p_n = \left[\epsilon_n^+ + \frac{(\epsilon_n^-)^2}{(E-t)-\epsilon_n^+} + \frac{4}{E-K}\right] p_n + \frac{2}{E-K}(p_{n-1}+p_{n+1}). \tag{25}$$

As a consequence of this choice, an extended state $\mathcal{D}$ exists at energy $E = K$, regardless of any other control parameters of Eq. (21):

$$E = K, \quad c_n = (-1)^n, \quad f_n = p_n = 0. \tag{26}$$

The state's amplitudes reside only on the c sites (see Fig. 6). The existence of this extended state is not affected by the perturbation strength λ, the flat-band energy $E = t$, and any specific correlation of the on-site potential. Therefore if the model admits a mobility edge curve $\lambda_c(E_c)$, it follows that it will diverge $\lambda_c(E_c = K) = \infty$, yielding a singularity.

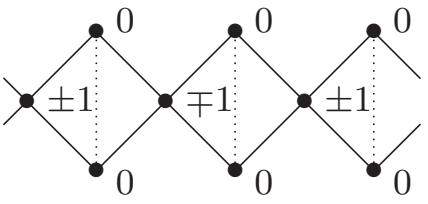

FIG. 6. Extended state $\mathcal{D}$ at energy $E = K$ on the diamond lattice in the case of constant on-site potential $\epsilon_n^c = K$ on the c chain (up to normalization).

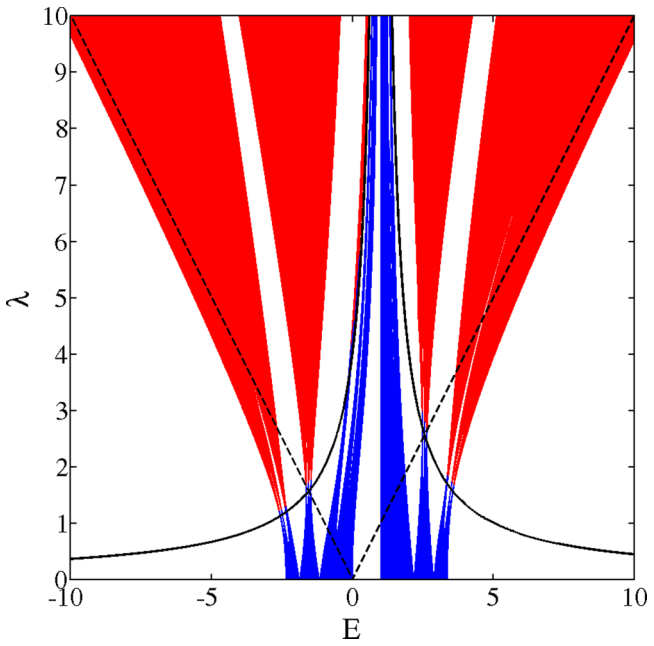

FIG. 7. (Color online) Symmetric case. Dispersive spectrum ($\sigma_{p,c}$) of the diamond lattice, for $\epsilon_n^- = 0$, $K = 1$, $t = 0$. The Fano state spectrum (σ_f) is omitted, but its boundaries are indicated by black dashed lines. The extended (localized) states of the dispersive spectrum are shown in blue (red); the boundary between these is a mobility edge approximation, in good agreement with the analytical form of Eq. (29), shown as a solid black line. Note that at $E = K$, the mobility edge diverges to infinity.

A. Symmetric case: Analytic mobility edge

We consider first the symmetric case $\epsilon_n^- = 0$, obtained for $\theta_b = 0.0$. In this situation, Eq. (21) reads

$$\begin{aligned}(E+t)\,p_n &= \epsilon_n^+\,p_n + -\sqrt{2}(c_n + c_{n+1}),\\ (E-t)\,f_n &= \epsilon_n^+\,f_n,\\ (E-K)\,c_n &= -\sqrt{2}(p_{n-1}+p_n).\end{aligned} \tag{27}$$

The f_n states decouple from both p_n and c_n states, generating two independent spectra σ_f and $\sigma_{p,c}$. The flat-band energy t shifts the two energy spectra of $2t$ relative to each other. The rotated Eq. (25) now turns into

$$\begin{aligned}\tilde{E}\,p_n &= \frac{(E-K)\lambda}{2}\cos(2\pi\alpha n)\,p_n + p_{n-1} + p_{n+1},\\ \text{where } \tilde{E} &:= \frac{(E+t)(E-K)}{2} - 2.\end{aligned} \tag{28}$$

Note that the on-site potential strength is now dependent on λ and E. Imposing the equality between the potential strength and the Aubry-André critical value, we arrive at the mobility edge

$$\left|\frac{(E_c-K)}{2}\lambda_c\right| = 2 \quad \Rightarrow \quad \lambda_c(E_c) = \left|\frac{4}{E_c-K}\right|. \tag{29}$$

The mobility edge curve diverges at $E = K$ due to the existence of the delocalized state $\mathcal{D}$. We plot this mobility edge curve in Fig. 7 and observe very good agreement with the numerical results.

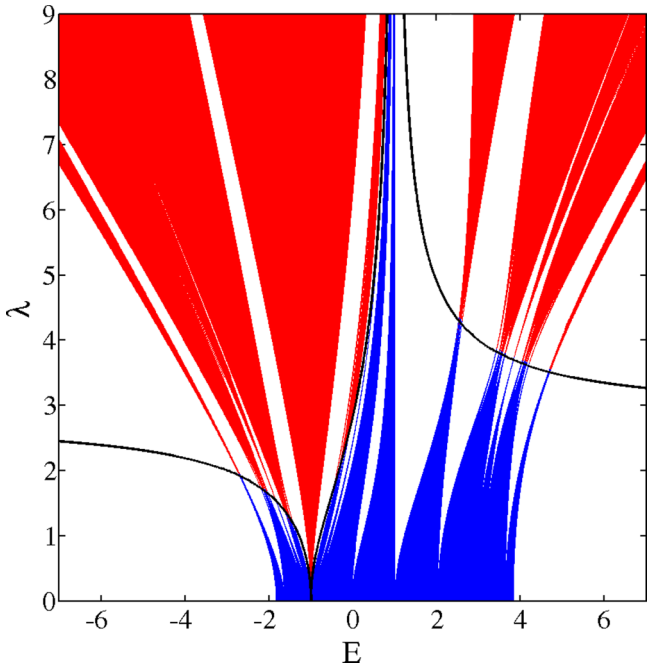

FIG. 8. (Color online) Antisymmetric case. Spectrum of the diamond lattice, for $\epsilon_n^+ = 0$, $K = 1$, $t = -1$. The extended (localized) spectral portion is shown in blue (red). The boundary between is an approximation of the spectrum's mobility edge—in good agreement with the analytical form of Eq. (32), plotted as a black line. Note that the mobility edge curve zeros at $E = t$, as well as diverges at $E = K$.

B. Antisymmetric case: Analytic mobility edge

We consider the antisymmetric case $\epsilon_n^+ = 0$ obtained with $\theta_b = 0.5$, and with $\epsilon_n^c = K$. Equation (21) reads

$$\begin{aligned}(E+t)\,p_n &= \epsilon_n^-\, f_n - \sqrt{2}(c_n + c_{n+1}),\\ (E-t)\,f_n &= \epsilon_n^-\, p_n,\\ (E-K)\,c_n &= -\sqrt{2}(p_{n-1} + p_n).\end{aligned} \tag{30}$$

For $t \neq K$, all eigenenergies are expelled from the flat-band energy $E = t$.

In Fig. 8 we plot the spectrum for this antisymmetric case for $t = -1$ and $K = 1$. We derive an analytical expression of the mobility edge by reducing Eq. (30) to an Aubry-André form for the p_n coordinates:

$$\tilde{E}\,p_n = \frac{E-K}{2}\frac{\lambda^2}{2(E-t)}\cos(4\pi\alpha n)\,p_n + p_{n-1} + p_{n+1},$$
$$\text{where } \tilde{E} := \frac{E-K}{2}\left[(E+t) - \frac{\lambda^2}{2(E-t)}\right] - 2. \tag{31}$$

The condition for the MIT yields

$$\left|\frac{E-K}{2}\frac{\lambda_c^2}{2(E-t)}\right| = 2 \;\Rightarrow\; \lambda_c(E) = 2\sqrt{2\left|\frac{E-t}{E-K}\right|}. \tag{32}$$

In Eq. (32), the mobility edge curve $\lambda_c(E_c)$ diverges to infinity at $E = K$, in correspondence to the delocalized state $\mathcal{D}$. The curve also displays a zero at $E = t$, which corresponds to the lack of any states at the flat-band energy [27]. The mobility edge curve of Eq. (32) is plotted in Fig. 8 and shows excellent agreement with the numerical data.

V. CONCLUSION

Flat-band topologies are characterized by macroscopic degeneracy at the flat-band energy. General perturbations of these topologies lead to a removal of the degeneracy, yet keep a high density of states and a bunching of the renormalized and hybridized states around the original flat-band energy. This has especially dramatic consequences for quasiperiodic Aubry-André form perturbations. The flat-band energy now hosts a zero of a mobility edge curve $\lambda_c(E_c)$. When approaching this zero the density of states grows, and the spatial extent of the eigenstates drops, making them more localized. For specific symmetries of the applied quasiperiodic potential, the dependence $\lambda_c(E_c)$ is obtained analytically, confirming the predicted zero, and further proving the strict nonexistence of any state at the former flat-band energy. Some flat-band topologies allow the existence of completely delocalized eigenstates at certain energies $E = K$. This leads to even more complex mobility edge curves which allow for a coexistence of zeros and divergencies of $\lambda_c(E_c)$. Possible future topics of study include extension to $U > 1$ topological classes and higher dimensional flat-band models. It is our hope that the use of flat-band topologies will contribute interest to tunable mobility edges, e.g., by those realized in graphene [28], monolayered dichalcogenides [29], or vanadium dioxide films [30].

[1] P. W. Anderson, Phys. Rev. **109**, 1492 (1958).
[2] B. R. Bulka, B. Kramer, and A. MacKinnon, Z. Phys. B: Condens. Matter **60**, 13 (1985).
[3] F. M. Izrailev and A. A. Krokhin, Phys. Rev. Lett. **82**, 4062 (1999).
[4] S. Aubry and G. André, Ann. Israel Phys. Soc. **3**, 133 (1980).
[5] A. Avila and S. Jitomirskaya, Ann. Math. **170**, 303 (2009).
[6] S. Jitomirskaya and I. V. Krasovsky, Math. Res. Lett. **9**, 413 (2002).
[7] A. Avila, arXiv:0810.2965.
[8] S. Jitomirskaya, Ann. Math. **150**, 1159 (1999).
[9] A. Gordon, S. Jitomirskaya, Y. Last, and B. Simon, Acta Math. **178**, 169 (1997).
[10] S. Ostlund, R. Pandit, D. Rand, H. J. Schellnhuber, and E. D. Siggia, Phys. Rev. Lett. **50**, 1873 (1983).
[11] M. Kohmoto, L. P. Kadanoff, and C. Tang, Phys. Rev. Lett. **50**, 1870 (1983).
[12] H. Hiramoto and M. Kohmoto, Phys. Rev. B **40**, 8225 (1989).
[13] D. J. Boers, B. Goedeke, D. Hinrichs, and M. Holthaus, Phys. Rev. A **75**, 063404 (2007).

[14] D. R. Grempel, S. Fishman, and R. E. Prange, Phys. Rev. Lett. **49**, 833 (1982).
[15] S. Flach, M. Ivanchenko, and R. Khomeriki, Europhys. Lett. **98**, 66002 (2012).
[16] S. Ganeshan, J. H. Pixley, and S. Das Sarma, Phys. Rev. Lett. **114**, 146601 (2015).
[17] F. Bloch, J. Dalibard, and W. Zwerger, Rev. Mod. Phys. **80**, 885 (2005).
[18] D. N. Christodoulides, F. Lederer, and D. Silberberg, Nature (London) **424**, 817 (2003).
[19] N. Masumoto, N. Kim, T. Burnes, K. Kusudo, A. Loeffler, S. Hoefling, A. Forchel, and Y. Yamamoto, New J. Phys. **14**, 065002 (2012).
[20] O. Derzhko and J. Richter, Eur. Phys. J. B **52**, 23 (2006).
[21] O. Derzhko, J. Richter, A. Honecker, M. Maksymenko, and R. Moessner, Phys. Rev. B **81**, 014421 (2010).
[22] D. Leykam, S. Flach, O. Bahat-Treidel, and A. S. Desyatnikov, Phys. Rev. B **88**, 224203 (2013).
[23] S. Flach, D. Leykam, J. D. Bodyfelt, P. Matthies, and A. S. Desyatnikov, Europhys. Lett. **105**, 30001 (2014); **106**, 19901 (2014).
[24] A. Honecker, F. Mila, and M. Troyer, Eur. Phys. J. B **15**, 227 (2000); T. Hakobyan, J. H. Hetherington, and M. Roger, Phys. Rev. B **63**, 144433 (2001); F. Casola *et al.*, Phys. Rev. Lett. **110**, 187201 (2013); T. Sugimoto, M. Mori, T. Tohyama, and S. Maekawa, JPS Conf. Proc. **3**, 014016 (2014).
[25] J. D. Bodyfelt, D. Leykam, C. Danieli, X. Yu, and S. Flach, Phys. Rev. Lett. **113**, 236403 (2014).
[26] We have varied this cutoff value up to $\xi \leqslant N$, and it does not change the spectra drastically.
[27] With a similar argument discussed in Sec. III, in this antisymmetry all the eigenstates are expelled from the flat-band energy $E = t$.
[28] L. A. Ponomarenko, A. K. Geim, A. A. Zhukov, R. Jalil, S. V. Morozov, K. S. Novoselov, I. V. Grigorieva *et al.*, Nat. Phys. **7**, 958 (2011).
[29] B. Radisavljevic and A. Kis, Nat. Mater. **12**, 815 (2013).
[30] J. Givernaud, C. Champeaux, A. Catherinot, A. Pothier, P. Blondy, and A. Crunteanu, in *2008 IEEE MTT-S International Microwave Symposium* (IEEE, Piscataway, 2008), p. 1103; F. Fan, Y. Hou, Z. Jiang, X. Wang, and S. Chang, Appl. Opt. **51**, 4589 (2012).